AMERICAN ACADEMY OF OPHTHALMOLOGY®

Peripapillary Choroidal Vascularity Index for Differentiating Papilledema from Pseudopapilledema: A Deep Learning–Based Approach

Nicola Valsecchi, MD,[1,2] *Lorenzo Padovani, MD,*[1,2] *Elli Davis, MD,*[3] *Mohammed Nasar Ibrahim, PhD,*[3] *Anna Elena Vallone, MD,*[1,2] *Matilde Roda, MD,*[1,2] *Maurizio Mete, MD,*[1,2] *Antonio Moramarco, MD,*[1,2] *Costantino Schiavi, MD, PhD,*[1,2] *Kiran Kumar Vupparaboina, PhD,*[3] *Jay Chhablani, MD,*[3] *Luigi Fontana, MD, PhD*[1,2]

Purpose: To compare the peripapillary choroidal vascularity index (PPCVI) in eyes with papilledema secondary to idiopathic intracranial hypertension (IIH) and pseudopapilledema due to optic disc drusen (ODD) using a novel deep learning algorithm.

Design: A retrospective observational cohort study.

Subjects: The study included 30 eyes of 15 patients with papilledema secondary to IIH, 30 eyes of 15 patients with ODD, and 78 eyes of 39 age- and sex-matched healthy controls. All cases of IIH and ODD were confirmed with lumbar puncture and B-scan ultrasonography, respectively.

Methods: OCT was performed using a 3.4 mm diameter 360° peripapillary circle scan. Choroidal segmentation was automatically performed with a deep learning ResUNet model and a volumetric smoothing algorithm. The choroidal vascularity index was quantified in each peripapillary scan. Statistical comparisons were made between groups and in IIH patients before and after resolution of papilledema. Linear mixed models were used for analysis.

Main Outcome Measures: Mean PPCVI, expressed as a percentage, across study groups and longitudinally in IIH eyes.

Results: There were no significant differences among groups regarding age, sex, visual acuity, or intraocular pressure ($P > 0.05$). Mean PPCVI was significantly reduced in the papilledema group compared with the pseudopapilledema and control groups (31.7% ± 8.4% vs. 39.0% ± 8.1% and 40.7% ± 5.6%, respectively; $P < 0.001$). After a mean follow-up of 36 ± 12.1 months, IIH patients with resolved papilledema showed a significant increase in PPCVI (34.8% ± 8.0% vs. 31.7% ± 8.4%, $P = 0.033$), although values remained lower compared with pseudopapilledema and control groups ($P < 0.001$).

Conclusions: Reduced PPCVI could be a potential biomarker for differentiating papilledema from pseudopapilledema. An increase in PPCVI after resolution of papilledema supports its utility as a potential parameter for monitoring disease activity.

Financial Disclosure(s): Proprietary or commercial disclosure may be found in the Footnotes and Disclosures at the end of this article. *Ophthalmology Science 2026;6:101024 © 2025 by the American Academy of Ophthalmology. This is an open access article under the CC BY-NC-ND license (http://creativecommons.org/licenses/by-nc-nd/4.0/).*

Supplemental material available at www.ophthalmiologyscence.org.

Papilledema refers to optic disc swelling caused by elevated intracranial pressure (IxCP).[1] The primary mechanism of vision loss in papilledema is likely due to axoplasmic flow stasis, as elevated ICP raises cerebrospinal fluid pressure around the optic nerves, disrupting the normal pressure gradient between intraocular and retrolaminar pressures.[2] Various conditions can lead to elevated ICP, including intracerebral mass lesions, cerebral hemorrhage, and hydrocephalus. Idiopathic intracranial hypertension (IIH) is a clinical syndrome characterized by increased ICP, normal cerebrospinal fluid, papilledema, and no alternative underlying etiology.[3] Idiopathic intracranial hypertension primarily affects obese women of childbearing age, with an estimated annual incidence of 0.9 per 100 000 in the general population and 3.5 per 100 000 among females aged 15–44 years.[4]

Pseudopapilledema is characterized by optic disc elevation without peripapillary fluid, most commonly resulting from optic disc drusen (ODD), though it can arise from various optic disc abnormalities.[2] It is a benign condition that does not involve elevated ICP and rarely poses a threat to vision.[5] Accurate differentiation between

https://doi.org/10.1016/j.xops.2025.101024
ISSN 2666-9145/25

papilledema and pseudopapilledema is critical, as papilledema may indicate potentially life-threatening conditions, whereas misdiagnosing pseudopapilledema as papilledema can lead to unnecessary diagnostic procedures. Despite advancements in imaging modalities, no single technique reliably distinguishes papilledema from pseudopapilledema, and previous studies indicated that >50% of children with pseudopapilledema may undergo unnecessary lumbar punctures.[6,7]

Recently, several studies explored the use of OCT in optic nerve diseases, highlighting its potential as a valuable diagnostic tool. Furthermore, artificial intelligence and deep learning systems have shown promising results in analyzing fundus photographs and reconstructions of the optic nerve head.[8] Despite efforts to study retinal biomarkers, there is limited understanding of choroidal changes in papilledema, and limited studies addressed peripapillary choroidal parameters in conditions related to the optic nerve.[9,10] Recently, Kaya and Arici observed a reduction in the peripapillary choroidal thickness in patients with IIH in both the acute and chronic stages compared with healthy individuals.[11] Also, Kesim et al[12] observed a significant decrease in the peripapillary choroidal vascularity index (PPCVI) in IIH compared with controls. However, to our knowledge, no previous studies attempted to compare the peripapillary choroid in papilledema and pseudopapilledema.

A fundamental limitation in evaluating choroidal parameters is the reliance on manual segmentation, which depends on the subjective interpretation of graders. To overcome this limitation, we developed a deep learning–based method to automatically assess the PPCVI from optic nerve OCT scans. The main objective of the present study was to assess PPCVI in eyes with papilledema and to compare these values with those from eyes with pseudopapilledema and healthy controls. Furthermore, we conducted a longitudinal assessment of PPCVI changes in patients with papilledema, evaluating measurements before and after disease resolution.

Methods

Study Population

This retrospective study was conducted at the University of Bologna (Italy) between January 2020 and October 2024. The study adhered to the ethical principles of the Declaration of Helsinki. All patients and healthy controls provided written informed consent for the use of their clinical and imaging data in this study. This study was approved by the Ethics Committee of Bologna, Italy (Cod CE: 53/2025/Oss/AOUBo). Patients with a confirmed diagnosis of IIH and ODD were included in the study. The diagnosis of IIH was based on modified Dandy–Walker criteria.[3] The severity of papilledema was graded according to Frisen classification, and patients with papilledema stage 2, stage 3, and stage 4 were included.[13] Patients with ODD were diagnosed using enhanced depth imaging OCT (Spectralis HRA + OCT; Heidelberg Engineering) following the guidelines from the Optic Disc Drusen Studies Consortium.[14] The inclusion criteria for the ODD group required the presence of visible or buried drusen, along with the absence of subjective visual symptoms and vascular complications. Furthermore, the diagnosis of ODD was confirmed using B-scan ultrasonography. The control group consisted of age- and sex-matched ophthalmology patients who exhibited normal findings in their fundoscopic examinations and who had no concomitant comorbidities. Both eyes were examined in all the participants. Patients diagnosed with papilledema secondary to IIH were evaluated both in the acute phase and after resolution of papilledema, defined by a normalization of the ophthalmoscopic characteristics of the optic nerve head and by a thickness of the retinal nerve fiber layer (RNFL) within normal limits.[15]

Exclusion criteria for all groups included a history of any systemic illness or concomitant ophthalmic diseases, high myopia (greater than −6 diopters), hyperopia (greater than +3 diopters), and astigmatism (greater than ±3 diopters), any condition impairing choroidal examination, previous ocular trauma, concomitant choroidal neovascularization, and prior ocular surgery and/or laser treatment.

Clinical Assessment

Demographic information and comprehensive medical and ophthalmic histories were collected during the initial visit. All participants underwent an ocular examination, which included best-corrected visual acuity assessment, Goldmann tonometry, slit lamp biomicroscopy, and fundoscopy. Furthermore, patients with papilledema secondary to IIH underwent a 24-2 Humphrey visual field test using the Humphrey Field Analyzer 3 (Carl Zeiss Humphrey Systems) both in the acute phase and after resolution of papilledema.

OCT Image Acquisitions

All OCT assessments were conducted using the Heidelberg Spectralis spectral-domain OCT (SD-OCT; Heidelberg Engineering). Acquisitions were performed between 13.00 and 15.00 to avoid diurnal variations. Images were acquired using a standard RNFL evaluation protocol, utilizing a 360° 3.4 mm diameter peripapillary circle scan. The RNFL thickness was assessed using the same peripapillary circle scans, and values for the mean, superior, inferior, temporal, and nasal regions were recorded. The peripapillary choroid was assessed using the same images. Both eyes of the same patients were used for the statistical analysis.

Assessment of the PPCVI Using the Novel Deep Learning–Based Approach

The proposed algorithm for analyzing PPCVI in OCT B-scans follows a multistep approach, including segmenting the choroidal layer and its vessels (see Fig 1). Segmentation of the choroidal layer involves identifying its boundaries with the retina and sclera, known as the choroidal inner boundary (CIB) and choroidal outer boundary (COB), respectively. While detecting the CIB is relatively straightforward in healthy eyes, it becomes more challenging in diseased eyes due to conditions like pigment epithelial detachments and drusen, which can distort the retinal pigment epithelium. On the other hand, identifying the COB is significantly more difficult because of the gradual intensity transitions at the interface.[16] Previous statistical and graph-based methods applied to diverse datasets have been both computationally intensive and frequently inaccurate.[17] However, recent machine learning approaches have shown improved accuracy and reduced latency.[18]

In this study, we utilized our previously validated deep learning model based on the residual U-Net (ResUNet) architecture for segmenting the choroidal layer in peripapillary scans.[18] Images were resized to 256 × 256 pixels, and the model was trained for 80 epochs with a batch size of 8, chosen based on preliminary

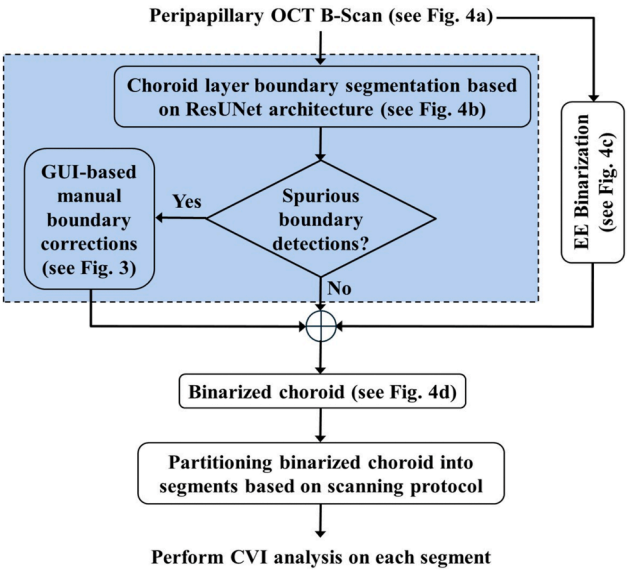

Figure 1. Workflow overview of the proposed method. CVI = choroidal vascularity index; EE = exponential enhancement; GUI = graphical user interface.

experiments to optimize convergence speed, training stability, and segmentation accuracy, as previously reported.[18] The deep learning model was initially validated on 50 peripapillary SD-OCT scans from healthy controls, achieving correct delineation of both the choroidal inner and outer boundaries in 95.8% of cases. Correct segmentation was defined as accurate boundary delineation without the need for manual correction, and all results were visually reviewed by a trained grader (E.D.) and confirmed by a second grader (N.V.). Subsequently, this deep learning method was applied in the present study. In brief, the ResUNet model generates a mask for the choroidal layer, as illustrated in Figure 2B. The upper and lower edges of this mask are then traced to determine the CIB and COB, which are overlaid on the original image (Fig 2C). When boundary detection errors occur, we employ a custom graphical user interface that allows for manual corrections by enabling users to mark sparse points along the boundaries. These points are then interpolated using a spline technique, as seen in Figure 2D–F. The highlighted section in Figure 1 outlines the complete process of identifying the choroidal boundaries, including automated detection of the CIB and COB, along with an option for manual correction. One trained grader (E.D.) performed the segmentation when manual correction was needed, masked to patients' characteristics. Then, the segmentation was revised by another trained grader (N.V.) for accuracy. In cases of inaccuracy, the segmentation was repeated. Overall, the algorithm demonstrated robust performance across different conditions, achieving accurate segmentation in 95.3% of healthy eyes, 94.6% of eyes with ODD, and 93.6% of eyes with papilledema. Manual correction was required for the remaining cases.

The next step involved detecting choroidal vessels within the choroidal layer, a task complicated by the intricate and densely packed structure of these vessels. Additionally, the OCT acquisition process introduces artifacts such as speckle noise and uneven intensity distribution. To tackle these issues, we employed a previously reported method that uses exponential enhancement and nonlinear equalization.[16,19] Exponential enhancement was applied to compensate for the exponential dynamic range compression and depth-dependent attenuation typical of OCT images, thereby improving contrast in the deeper choroidal layers. Nonlinear equalization was subsequently performed to normalize local brightness and enhance regional contrast uniformity. This enhancement facilitates better differentiation between vessel and nonvessel areas in the choroid, as depicted in Figure 3C, where vessels appear as dark regions in the binarized peripapillary image.[20] The enhanced image was then binarized using Phansalkar local adaptive thresholding method, which computes a threshold for each pixel based on the local mean and standard deviation within a small neighborhood, allowing robust separation of luminal choroidal areas (LCAs) (dark) from stromal choroidal areas (bright) even in low-contrast or noisy B-scans, as previously described.[21] Finally, using the CIB and COB detections from the first step (Fig 3B), we extract the binarized choroid (Fig 3D) from the peripapillary image (Fig 3C). The choroidal vascularity index (CVI) was calculated as the ratio of the LCA to the total choroidal area (TCA). According to the CVI analysis protocol, the binarized choroid is then segmented into 4 regions—nasal, temporal, superior, and inferior. For each segment, statistics such as mean, minimum, maximum, and standard deviation of CVI are computed for analysis.

Statistical Analysis

The Shapiro–Wilk test was used to assess normality, and parametric tests were employed for data analysis. Descriptive statistics are presented as mean ± standard deviation. Data from both eyes of each patient were included, and linear mixed models were applied to account for within-subject correlation when comparing RNFL and PPCVI among patients with IIH, ODD, and healthy controls. Pearson correlation analysis was performed to evaluate the relationships between choroidal parameters and functional outcomes, including visual field mean deviation, pattern standard deviation, and visual acuity. Paired *t* tests were performed to assess whether differences between right and left eyes were statistically significant within each group. Absolute intereye differences were subsequently compared across the 3 groups using 1-way analysis of variance to evaluate variability at the group level. Receiver operating characteristic curves were created to assess the ability of RNFL, PPCVI, and their combined effect to differentiate papilledema from pseudopapilledema and papilledema from controls. A significance level of $P < 0.05$ was applied. Statistical analyses were conducted using IBM SPSS version 26.

Results

Demographic Data

A total of 30 eyes of 15 patients with papilledema secondary to IIH, 30 eyes of 15 patients with pseudopapilledema secondary to ODD, and 78 eyes of 39 age- and sex-matched healthy controls were included. No differences in terms of age, sex, visual acuity, intraocular pressure, and spherical equivalent were observed between the 3 groups ($P > 0.05$). See Table 1. In the IIH group, 4 patients had stage 2 papilledema, 8 patients had stage 3, and 3 patients had stage 4 according to Frisen classification.[13] The mean follow-up duration for the resolved papilledema group was 36.0 ± 12.1 months (range: 24–49 months). Peripapillary SD-OCT scans were acquired. Peripapillary RNFL measurements were significantly increased in every quadrant in eyes with papilledema compared with pseudopapilledema and healthy eyes ($P < 0.001$) (see Supplementary file 1, available at www.ophthalmologyscience.org). On the other hand, no

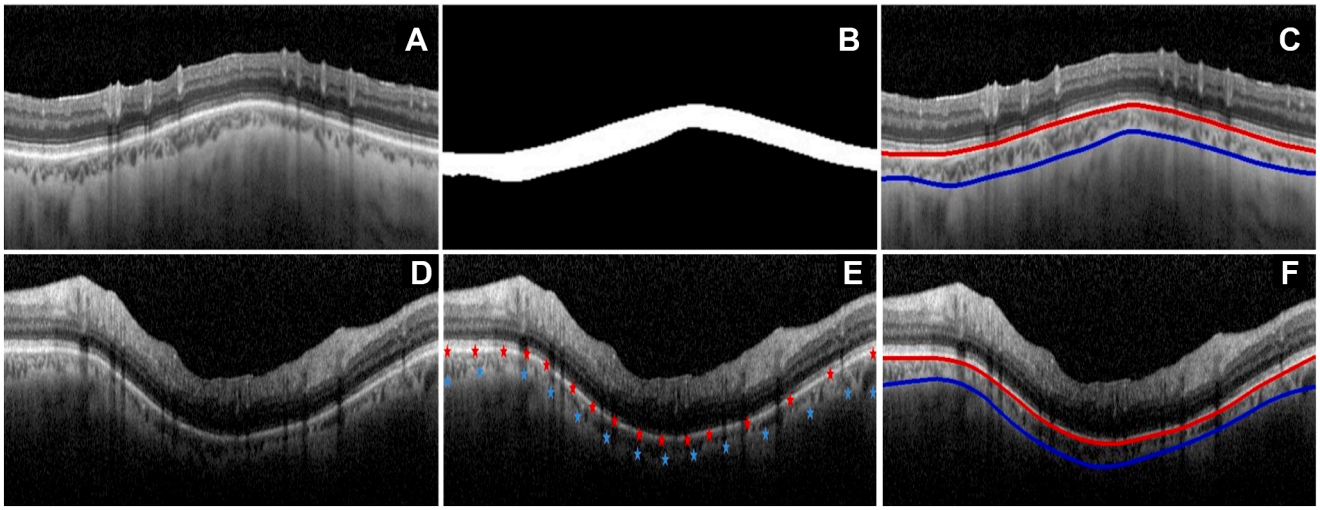

Figure 2. Steps in choroid layer boundary segmentation using ResUNet architecture. (**A**) Representative peripapillary image. (**B**) Choroid layer mask from ResUNet model output. (**C**) Choroidal inner boundary and COB overlaid on (**A**). (**D**) Applications of the manual boundary correction through inbuilt developed graphical user interface (GUI) on a representative peripapillary OCT B-scan. (**E**) Manually marked sparse points on choroid layer boundary through inbuilt developed GUI. (**F**) Choroidal inner boundary and COB detection based on spline interpolation. COB = choroidal outer boundary.

significant differences were observed among resolved papilledema, pseudopapilledema, and controls, except for a significant reduction of the nasal RNFL thickness in the resolved papilledema group ($P = 0.031$) (see Supplementary file 2, available at www.ophthalmologyscience.org). In longitudinal analysis, RNFL measurements in the resolved papilledema group were significantly reduced in all quadrants compared with the same eyes during the acute phase of IIH ($P < 0.001$) (see Supplementary file 3, available at www.ophthalmologyscience.org).

PPCVI Assessment

The mean PPCVI (%) was 31.7 ± 8.4 for the papilledema group, 39.0 ± 8.1 for the pseudopapilledema group, and 40.7 ± 5.6 for the control group ($P < 0.001$). The PPCVI values in all quadrants were significantly lower in the papilledema group compared with the pseudopapilledema and control groups ($P < 0.001$ for all quadrants). Furthermore, the mean peripapillary LCA values for the 4 quadrants were also significantly lower in the papilledema group compared with the pseudopapilledema and control groups ($P < 0.001$). The mean peripapillary TCA was also significantly lower in the papilledema group compared with the pseudopapilledema and control groups ($P < 0.05$), except for the nasal quadrant ($P > 0.05$) (see Table 2). Representative examples are shown in Figure 4. We did not observe a correlation between the mean PPCVI and the degree of papilledema ($r = -0.801$, $P = 0.648$). In longitudinal comparisons of IIH before and after papilledema resolution, eyes with resolved papilledema presented a mean increase in the PPCVI compared with the acute phase (34.8% ± 8.0% vs. 31.7% ± 8.4%, $P = 0.033$) (see Table 3). Representative examples are in Figure 5. Additionally, eyes with resolved papilledema presented a significant reduction in CVI, LCA, and TCA in all quadrants compared with controls and pseudopapilledema groups ($P < 0.05$) (see Table 4).

Intereye Variability

Paired comparisons between right and left eyes revealed no significant intereye differences for mean RNFL (right eye: 110.96 ± 54.24 µm; left eye: 109.93 ± 49.64 µm, $P = 0.727$), TCA (right eye: 2.02 ± 0.54 mm^2; left eye: 2.04 ± 0.51 mm^2, P=0.560), stromal choroidal area (right eye: 1.23 ± 0.38 mm^2; left eye: 1.23 ± 0.35 mm^2, $P = 0.936$), LCA (right eye: 0.76 ± 0.24 mm^2; left eye: 0.78 ± 0.25 mm^2, $P = 0.250$), and CVI (right eye: 38.16 ± 7.59%; left eye: 38.64 ± 7.98%, $P = 0.467$). One-way analysis of variance showed no significant differences in intereye variability among the 3 groups (controls, papilledema, and pseudopapilledema) for any parameter (RNFL, $P = 0.783$; TCA, $P = 0.949$; stromal choroidal area, $P = 0.670$; LCA, P=0.209; CVI, $P = 0.406$) (see Supplementary file 4, available at www.ophthalmologyscience.org). Scatter plots showing the intereye variations across all 3 groups are shown in Supplemental Figure 1, available at www.ophthalmologyscience.org.

RNFL, PPCVI, and Clinical Parameters in IIH Eyes

Eyes with IIH showed significant improvement in best-corrected visual acuity (pre 0.21 ± 0.11, post 0.01 ± 0.04, $P = 0.007$), mean deviation (pre −8.52 ± 3.61, post −5.49 ± 2.67 decibels, $P = 0.013$), and pattern standard deviation (pre 18.61 ± 8.23, post = 6.81 ± 2.34 decibels, $P = 0.021$) after resolution of

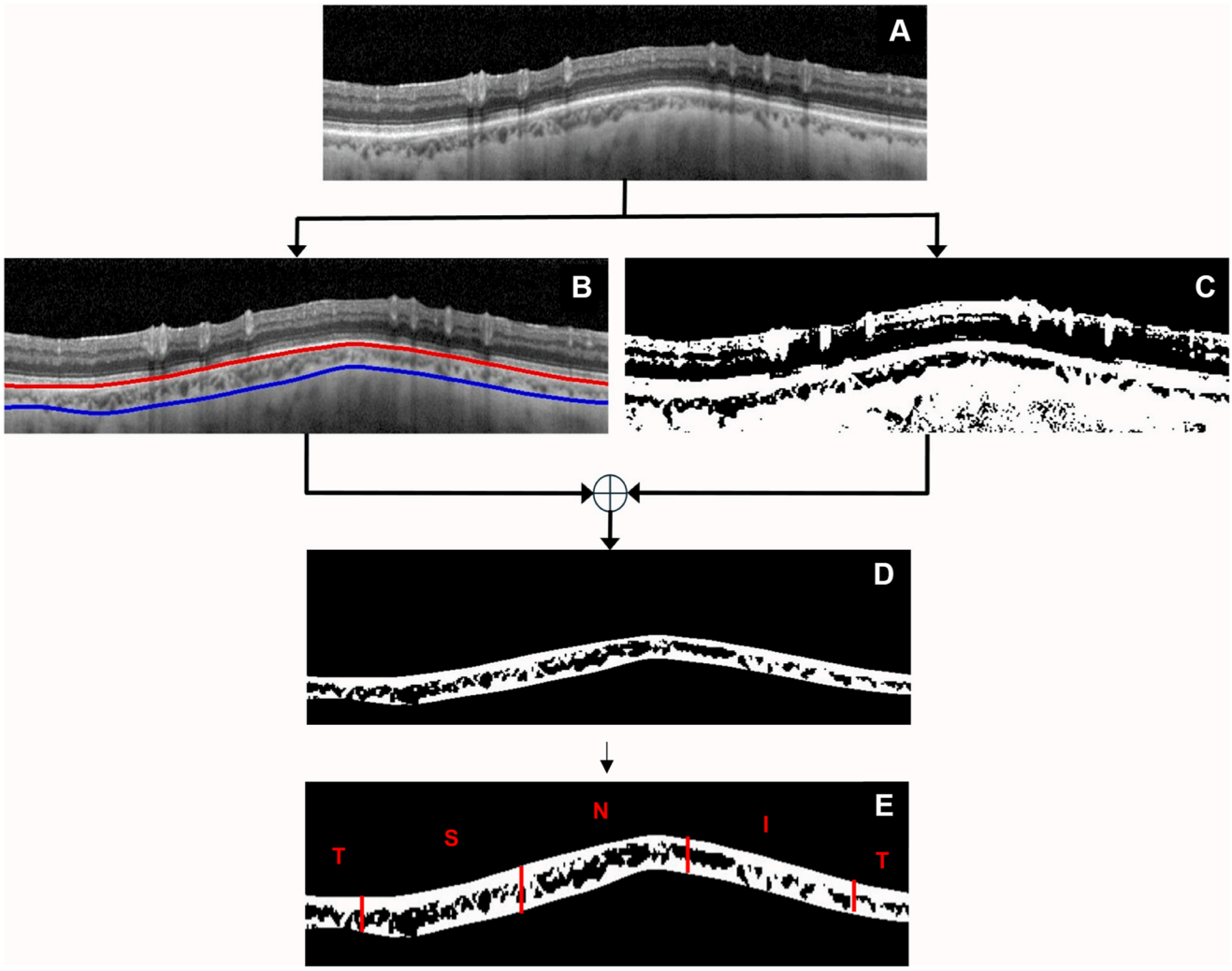

Figure 3. Graphical overview of the proposed method. (**A**) Representative peripapillary image. (**B**) Choroidal inner boundary and choroidal outer boundary detections. (**C**) Binarized peripapillary image. (**D**) Extraction of the binarized choroid. (**E**) The binarized choroid was segmented into 4 regions—temporal (T), superior (S), nasal (N), and inferior (I)—according to the standard protocol for retinal nerve fiber layer assessment.

papilledema. No significant correlations were observed between mean PPCVI and best-corrected visual acuity, mean deviation, or pattern standard deviation at baseline ($r = 0.061$, $P = 0.753$; $r = -0.157$, $P = 0.475$; $r = 0.168$, $P = 0.440$, respectively), or between mean RNFL and the same clinical parameters ($r = -0.187$, $P = 0.332$; $r = 0.286$, $P = 0.175$; $r = -0.115$, $P = 0.594$, respectively). Similarly, no significant associations were found when comparing mean PPCVI ($r = -0.174$, $P = 0.224$; $r = 0.132$, $P = 0.130$; $r = 0.014$, $P = 0.653$, respectively)

Table 1. Patient Demographics and Ophthalmic Findings in Study Groups

Demographic Data	Controls (n = 39)	IIH (n = 15)	ODD (n = 15)	*P* Value
Age (yrs), mean ± SD (CI)	31.3 ± 13.6 (26.9–35.7)	38.0 ± 18.0 (28–48)	29.2 ± 14.5 (21.1–37.3)	0.337
Sex, female (%)	30 (76.9%)	13 (86.6%)	10 (66.6%)	0.431
BCVA (logMAR), mean ± SD	0	0.1 ± 0.1	0	0.243
IOP (mmHg), mean ± SD (CI)	16.3 ± 2.9 (15.4–17.2)	17.1 ± 3.1 (15.4–18.8)	16.6 ± 2.8 (15.0–18.2)	0.843
Spherical equivalent (D), mean ± SD (CI)	+0.5 ± 1.8 (−0.08 to 1.08)	+1 ± 1.3 (0.28–1.72)	+0.4 ± 1.2 (−0.26 to 1.06)	0.645

BCVA = best-corrected visual acuity; CI = confidence interval; D = diopters; IIH = idiopathic intracranial hypertension; IOP = intraocular pressure; logMAR = logarithm of the minimum angle of resolution; ODD = optic disc drusen; SD = standard deviation.

Table 2. Peripapillary Choroidal Vascular Measurements in Eyes with Acute Papilledema Secondary to IIH, ODD, and Controls

Choroidal Parameters	Controls (n = 78)	Acute IIH (n = 30)	ODD (n = 30)	P Value
Mean, mean ± SD (CI)				
LCA, mm^2	0.84 ± 0.20 (0.79–0.89)	0.55 ± 0.12 (0.50–0.60)	0.78 ± 0.29 (0.67–0.89)	**<0.001**
SCA, mm^2	1.25 ± 0.38 (1.16–1.34)	1.23 ± 0.33 (1.10–1.35)	1.19 ± 0.34 (1.06–1.32)	0.718
CVI (%)	40.7% ± 5.6% (39.4–41.9)	31.7% ± 8.4% (28.5–34.8)	39.0% ± 8.1% (0.36–0.42)	**<0.001**
TCA, mm^2	2.13 ± 0.54 (2.01–2.26)	1.81 ± 0.35 (1.68–1.95)	2.01 ± 0.56 (1.80–2.22)	**0.019**
Temporal, mean ± SD (CI)				
LCA, mm^2	0.20 ± 0.05 (0.18–0.21)	0.13 ± 0.05 (0.11–0.15)	0.17 ± 0.07 (0.14–0.20)	**<0.001**
SCA, mm^2	0.33 ± 0.10 (0.31–0.35)	0.31 ± 0.10 (0.27–0.35)	0.31 ± 0.10 (0.27–0.35)	0.604
CVI (%)	38.0% ± 7% (36.4–39.6)	29.4% ± 11.6% (25.0–33.8)	34.0% ± 11% (31.5–37.9)	**<0.001**
TCA, mm^2	0.54 ± 0.13 (0.51–0.57)	0.45 ± 0.11 (0.41–0.50)	0.50 ± 0.15 (0.44–0.56)	**0.012**
Superior, mean ± SD (CI)				
LCA, mm^2	0.22 ± 0.05 (0.21–0.23)	0.14 ± 0.03 (0.13–0.15)	0.21 ± 0.07 (0.18–0.24)	**<0.001**
SCA, mm^2	0.33 ± 0.10 (0.31–0.36)	0.32 ± 0.09 (0.29–0.36)	0.32 ± 0.09 (0.28–0.36)	0.789
CVI (%)	40.2% ± 6.2% (38.8–41.6)	31.4% ± 7.7% (0.28.4–34.3)	39.1% ± 7.6% (36.2–41.8)	**<0.001**
TCA, mm^2	0.57 ± 0.14 (0.53–0.60)	0.48 ± 0.10 (0.44–0.51)	0.54 ± 0.15 (0.48–0.60)	**0.015**
Nasal, mean ± SD (CI)				
LCA, mm^2	0.22 ± 0.06 (0.21–0.24)	0.14 ± 0.03 (0.13–0.16)	0.21 ± 0.08 (0.18–0.24)	**<0.001**
SCA, mm^2	0.29 ± 0.10 (0.27–0.32)	0.30 ± 0.09 (0.27–0.34)	0.28 ± 0.09 (0.24–0.31)	0.639
CVI (%)	43.6% ± 6.6% (42.1–45.2)	33.9% ± 8.8% (30.5–37.3)	42.4% ± 8.0% (39.4–45.5)	**<0.001**
TCA, mm^2	0.53 ± 0.15 (0.50–0.56)	0.46 ± 0.10 (0.42–0.45)	0.50 ± 0.16 (0.44–0.56)	0.095
Inferior, mean ± SD (CI)				
LCA, mm^2	0.19 ± 0.05 (0.18–0.20)	0.12 ± 0.03 (0.11–0.14)	0.17 ± 0.07 (0.15–0.20)	**<0.001**
SCA, mm^2	0.28 ± 0.10 (0.26–0.30)	0.27 ± 0.08 (0.24–0.31)	0.26 ± 0.08 (0.23–0.30)	0.663
CVI (%)	41% ± 6.6% (39.8–42.8)	31.9% ± 10.2% (28.1–35.8)	39.7% ± 10.3% (35.9–43.6)	**<0.001**
TCA, mm^2	0.48 ± 0.15 (0.45–0.52)	0.41 ± 0.09 (0.37–0.44)	0.45 ± 0.12 (0.40–0.50)	**0.049**

Significant *P* values are highlighted in bold.
CI = confidence interval; CVI = choroidal vascularity index; IIH = idiopathic intracranial hypertension; LCA = luminal choroidal area; ODD = optic disc drusen; SCA = stromal choroidal area; SD = standard deviation; TCA = total choroidal area.

or mean RNFL ($r = -0.187$, $P = 0.332$; $r = 0.377$, $P = 0.080$; $r = -0.532$, $P = 0.060$, respectively) with these clinical parameters after resolution of papilledema.

Receiver Operating Characteristic Curves

Receiver operating characteristic curve analysis was performed to evaluate the diagnostic performance of mean RNFL and mean PPCVI. Individually, mean RNFL and mean PPCVI discriminated papilledema from pseudopapilledema (area under the curve [AUC] = 0.802, cutoff = 118.52 μm, $P < 0.001$; AUC = 0.740, cutoff = 33.25%, $P < 0.001$, respectively). Similarly, both parameters distinguished papilledema from healthy controls (AUC = 0.845, cutoff = 117.51, $P < 0.001$; AUC = 0.829, cutoff 35.42%, $P < 0.001$, respectively). Importantly, the combination of RNFL and PPCVI further enhanced diagnostic performance, achieving AUCs of 0.825 for papilledema versus pseudopapilledema and 0.887 for papilledema versus controls ($P < 0.001$) (see Fig 6).

Discussion

This study investigated the peripapillary choroidal vasculature in patients with papilledema, using a novel deep learning algorithm based on image binarization applied to peripapillary SD-OCT scans. The main result of this study was a significant reduction in PPCVI in eyes with papilledema compared with both pseudopapilledema and healthy control groups. Furthermore, papilledema resolution was associated with an increase in PPCVI.

Our study highlights the potential of a deep learning–based methodology for quantitative assessment of the peripapillary choroidal vasculature in optic nerve diseases. Although deep learning techniques have been widely implemented in OCT image analysis, their use has largely focused on the macula, with limited investigation of the peripapillary choroidal region. Our findings indicate that deep learning algorithms can provide highly accurate, reproducible, and efficient measurements of choroidal vascular parameters in optic nerve diseases. Furthermore, our results suggest that a reduction in PPCVI could be a promising biomarker in distinguishing between papilledema and pseudopapilledema.

Thickness of RNFL has been consistently reported to be greater in eyes with papilledema than in those with pseudopapilledema. In pediatric populations, Thompson et al reported excellent diagnostic accuracy for average RNFL thickness (AUC = 0.97), while Chiu et al found AUCs ranging from 0.81 to 0.90.[22,23] Among adults, Fard et al observed higher RNFL values in mild papilledema (AUC = 0.82), and Sekhri et al reported an AUC of 0.74 for global RNFL.[24,25] Recently, Girard et al[26] achieved an AUC of 0.99 using artifical intelligence models incorporating ODD and prelaminar volume parameters from OCT volumes of the optic nerve head to differentiate papilledema from ODD. However, their models did not include RNFL thickness or choroidal

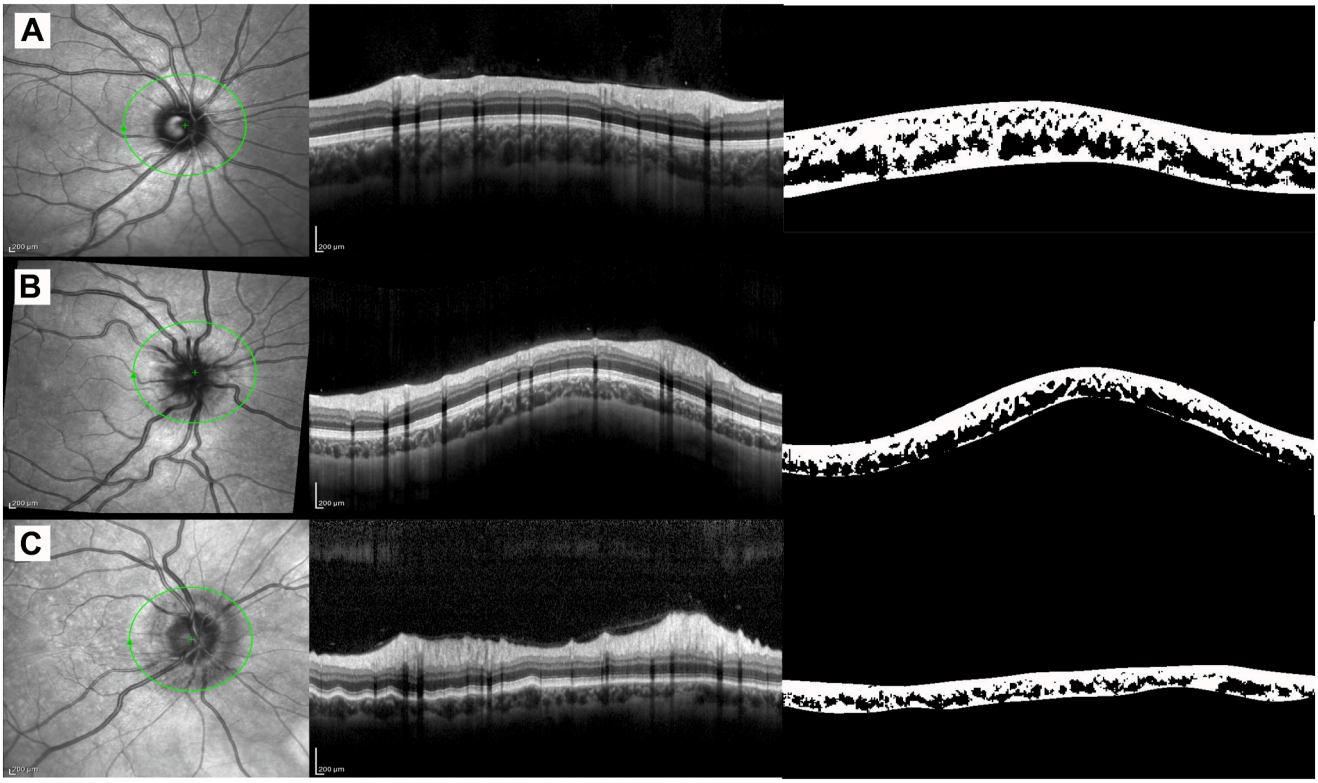

Figure 4. Peripapillary OCT in eyes of a healthy patient, patient with optic disc drusen, and a patient with papilledema secondary to IIH. (**A**) Note the peripapillary OCT B-scan showing a normal choroid in a 28-year-old female. Mean peripapillary CVI was 40.1%, whereas mean RNFL thickness was 94.53 μm. (**B**) Optic disc drusen eye in a 24-year-old female with a mean peripapillary CVI of 38.9% and a mean RNFL thickness of 98.44 μm. (**C**) OCT image in a 21-year-old female patient with stage 2 papilledema secondary to IIH. Mean peripapillary CVI was 32.3%, whereas mean RNFL thickness was 139.89 μm. This represents an easier scenario for segmentation and binarization of the peripapillary choroid. CVI = choroidal vascularity index; IIH = idiopathic intracranial hypertension; RNFL = retinal nerve fiber layer.

parameters. In the present study, both mean RNFL and mean PPCVI distinguished papilledema from pseudopapilledema (AUC = 0.802 and 0.740, respectively) and papilledema from controls (AUC = 0.845 and 0.829, respectively), using a standard single 360°, 3.4 mm diameter peripapillary circle scan. Notably, combining these parameters further improved diagnostic performance, achieving AUCs of 0.825 for differentiating papilledema from pseudopapilledema and 0.887 for differentiating papilledema from controls. These results suggest that incorporating PPCVI into artificial intelligence-based diagnostic models may enhance differentiation of papilledema from pseudopapilledema, even when using single peripapillary circle scans, potentially improving clinical decision-making in routine practice.

Previous studies have demonstrated impaired choroidal vasculature in papilledema, characterized by reduced blood flow in the peripapillary choroidal vessels. Using OCT angiography, Tüntaş Bilen and Atilla observed a significant reduction in peripapillary vessel density in IIH patients with papilledema compared with healthy controls.[27] Also, Kesim et al[12] observed a reduction in peripapillary CVI in eyes with papilledema compared with healthy controls. The vascular supply of the optic nerve head consists of 4 distinct layers: anteriorly, the radial peripapillary capillaries, which are perfused centrifugally by arterioles branching from the central retinal artery; the prelaminar vascular network, arising from peripapillary choroidal vessels supplied by the short posterior ciliary arteries; the laminar vasculature, formed by short posterior ciliary arteries that give rise to the circle of Zinn-Haller at the intrascleral level; and, posteriorly, the retrolaminar vascular layer, composed of anastomoses between short posterior ciliary arteries and vessels of the pia mater.[28,29] The peripapillary choroid is predominantly supplied by the short posterior ciliary arteries, which also contribute to the prelaminar network. In conditions of increased ICP, Mittra et al demonstrated significantly reduced blood flow velocities in the ophthalmic, short posterior ciliary, and central retinal arteries compared with healthy controls; these parameters improved substantially after optic nerve sheath decompression, as assessed by color Doppler imaging.[30] Therefore, reduction of PPCVI in papilledema could be partially explained by a reduction of blood flow in the short posterior ciliary arteries. Furthermore, parasympathetic and sympathetic innervation regulate choroidal blood flow, responding to retinal activity and systemic blood pressure fluctuations. Patients with papilledema have been reported to exhibit increased cerebral blood volume despite reduced cerebral blood

Table 3. Peripapillary Choroidal Vascular Measurements in Eyes with Acute and Resolved Papilledema Secondary to IIH

Choroidal Parameters	Acute IIH (n = 30)	Resolved IIH (n = 30)	*P* Value
Mean, mean ± SD (CI)			
LCA, mm^2	0.55 ± 0.12 (0.50–0.60)	0.57 ± 0.16 (0.51–0.63)	0.390
SCA, mm^2	1.23 ± 0.33 (1.10–1.35)	1.09 ± 0.34 (0.96–1.22)	**0.037**
CVI (%)	31.7% ± 8.4% (28.5–34.8)	34.8% ± 8.0% (31.8–37.9)	**0.033**
TCA, mm^2	1.81 ± 0.35 (1.68–1.95)	1.70 ± 0.41 (1.54–1.85)	0.114
Temporal, mean ± SD (CI)			
LCA, mm^2	0.13 ± 0.05 (0.11–0.15)	0.13 ± 0.05 (0.11–0.15)	0.954
SCA, mm^2	0.31 ± 0.10 (0.27–0.35)	0.28 ± 0.09 (0.25–0.32)	0.129
CVI (%)	29.4% ± 11.6% (25.0–33.8)	31.5% ± 10.2% (27.6–35.4)	0.182
TCA, mm^2	0.45 ± 0.11 (0.41–0.50)	0.42 ± 0.11 (0.38–0.46)	0.191
Superior, mean ± SD (CI)			
LCA, mm^2	0.14 ± 0.03 (0.13–0.15)	0.14 ± 0.04 (0.13–0.16)	0.714
SCA, mm^2	0.32 ± 0.09 (0.29–0.36)	0.28 ± 0.09 (0.25–0.32)	**0.021**
CVI (%)	31.4% ± 7.7% (0.28.4–34.3)	34.6% ± 7.1% (31.9–37.3)	**0.020**
TCA, mm^2	0.48 ± 0.10 (0.44–0.51)	0.44 ± 0.11 (0.39–0.48)	0.076
Nasal, mean ± SD (CI)			
LCA, mm^2	0.14 ± 0.03 (0.13–0.16)	0.16 ± 0.05 (0.14–0.18)	**0.021**
SCA, mm^2	0.30 ± 0.09 (0.27–0.34)	0.26 ± 0.09 (0.23–0.30)	**0.015**
CVI (%)	33.9% ± 8.8% (30.5–37.3)	38.6% ± 8.2% (35.5–41.8)	**0.007**
TCA, mm^2	0.46 ± 0.10 (0.42–0.45)	0.44 ± 0.12 (0.39–0.48)	0.174
Inferior, mean ± SD (CI)			
LCA, mm^2	0.12 ± 0.03 (0.11–0.14)	0.12 ± 0.03 (0.11–0.14)	0.777
SCA, mm^2	0.27 ± 0.08 (0.24–0.31)	0.25 ± 0.08 (0.21–0.28)	0.145
CVI (%)	31.9% ± 10.2% (28.1–35.8)	34.4% ± 9.5% (30.7–38.0)	0.194
TCA, mm^2	0.41 ± 0.09 (0.37–0.44)	0.39 ± 0.09 (0.35–0.42)	0.206

Significant *P* values are highlighted in bold.
CI = confidence interval; CVI = choroidal vascularity index; IIH = idiopathic intracranial hypertension; LCA = luminal choroidal area; SCA = stromal choroidal area; SD = standard deviation; TCA = total choroidal area.

flow.[31,32] Hence, reduced systemic volume and pressure in conditions of increased ICP could trigger sympathetic-mediated vasoconstriction of the choroidal vasculature, contributing to a decline in the PPCVI. Additionally, delayed circulation within the peripapillary choroid has been observed, likely due to venous stasis caused by compression of the thin-walled, low-pressure venous channels in this region.[33] This vascular compression is

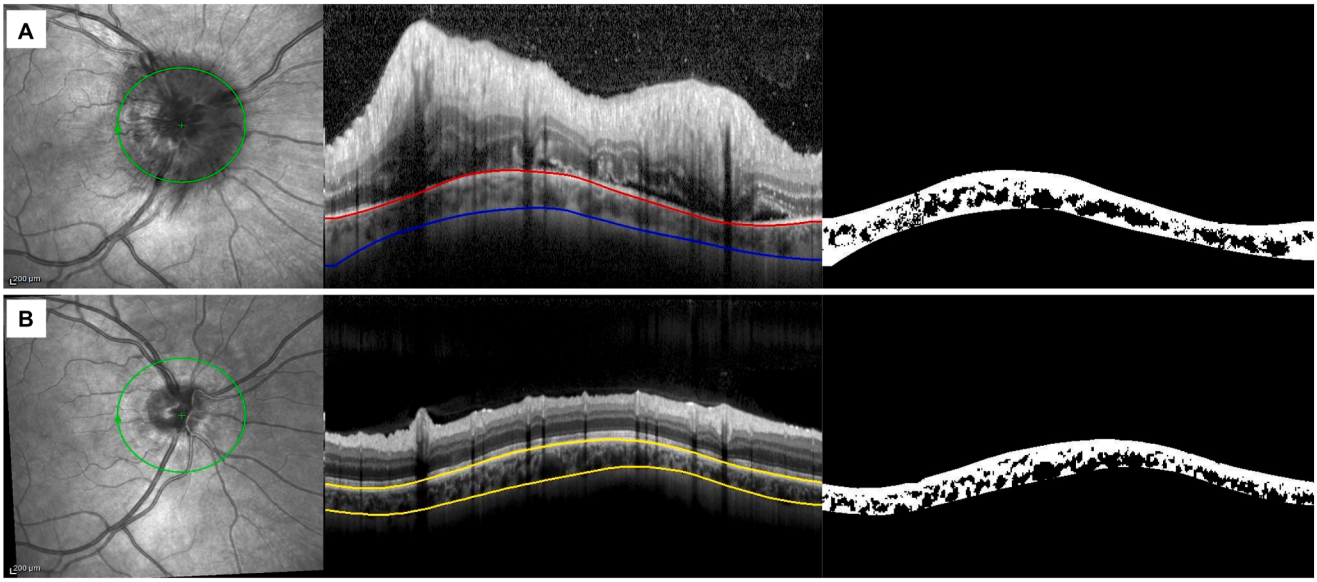

Figure 5. Peripapillary CVI before and after resolution of papilledema. (**A**) A 35-year-old female with stage 4 papilledema secondary to IIH in the right eye. Intracranial pressure was 32 cmH2O. Note the presence of subretinal fluid in the peripapillary area, engorged retinal vessels, and increased RNFL thickness. This represents a challenging case for segmentation and binarization of the peripapillary choroid. (**B**) After 30 months from the acute phase, the patient presented an increase in the peripapillary CVI and a reduction in the RNFL thickness (32.4% vs. 35.8% and 189.91 μm vs. 93.60 μm, respectively). CVI = choroidal vascularity index; IIH = idiopathic intracranial hypertension; RNFL = retinal nerve fiber layer.

Table 4. Peripapillary Choroidal Vascular Measurements in Eyes with Resolved Papilledema Secondary to IIH, ODD, and Controls

Choroidal Parameters	Controls (n = 78)	Resolved IIH (n = 30)	ODD (n = 30)	*P* Value
Mean, mean ± SD (CI)				
LCA, mm^2	0.84 ± 0.20 (0.79–0.89)	0.57 ± 0.16 (0.51–0.63)	0.78 ± 0.29 (0.67–0.89)	**<0.001**
SCA, mm^2	1.25 ± 0.38 (1.16–1.34)	1.09 ± 0.34 (0.96–1.22)	1.19 ± 0.34 (1.06–1.32)	0.126
CVI (%)	40.7% ± 5.6% (39.4–41.9)	34.8% ± 8.0% (31.8–37.9)	39.0% ± 8.1% (0.36–0.42)	**0.001**
TCA, mm^2	2.13 ± 0.54 (2.01–2.26)	1.70 ± 0.41 (1.54–1.85)	2.01 ± 0.56 (1.80–2.22)	**0.001**
Temporal, mean ± SD (CI)				
LCA, mm^2	0.20 ± 0.05 (0.18–0.21)	0.13 ± 0.05 (0.11–0.15)	0.17 ± 0.07 (0.14–0.20)	**<0.001**
SCA, mm^2	0.33 ± 0.10 (0.31–0.35)	0.28 ± 0.09 (0.25–0.32)	0.31 ± 0.10 (0.27–0.35)	0.087
CVI (%)	38.0% ± 7% (36.4–39.6)	31.5% ± 10.2% (27.6–35.4)	34.0% ± 11% (31.5–37.9)	**0.003**
TCA, mm^2	0.54 ± 0.13 (0.51–0.57)	0.42 ± 0.11 (0.38–0.46)	0.50 ± 0.15 (0.44–0.56)	**<0.001**
Superior, mean ± SD (CI)				
LCA, mm^2	0.22 ± 0.05 (0.21–0.23)	0.14 ± 0.04 (0.13–0.16)	0.21 ± 0.07 (0.18–0.24)	**<0.001**
SCA, mm^2	0.33 ± 0.10 (0.31–0.36)	0.28 ± 0.09 (0.25–0.32)	0.32 ± 0.09 (0.28–0.36)	0.064
CVI (%)	40.2% ± 6.2% (38.8–41.6)	34.6% ± 7.1% (31.9–37.3)	39.1% ± 7.6% (36.2–41.8)	**0.001**
TCA, mm^2	0.57 ± 0.14 (0.53–0.60)	0.44 ± 0.11 (0.39–0.48)	0.54 ± 0.15 (0.48–0.60)	**<0.001**
Nasal, mean ± SD (CI)				
LCA, mm^2	0.22 ± 0.06 (0.21–0.24)	0.16 ± 0.05 (0.14–0.18)	0.21 ± 0.08 (0.18–0.24)	**<0.001**
SCA, mm^2	0.29 ± 0.10 (0.27–0.32)	0.26 ± 0.09 (0.23–0.30)	0.28 ± 0.09 (0.24–0.31)	0.317
CVI (%)	43.6% ± 6.6% (42.1–45.2)	38.6% ± 8.2% (35.5–41.8)	42.4% ± 8.0% (39.4–45.5)	**0.009**
TCA, mm^2	0.53 ± 0.15 (0.50–0.56)	0.44 ± 0.12 (0.39–0.48)	0.50 ± 0.16 (0.44–0.56)	**0.018**
Inferior, mean ± SD (CI)				
LCA, mm^2	0.19 ± 0.05 (0.18–0.20)	0.12 ± 0.03 (0.11–0.14)	0.17 ± 0.07 (0.15–0.20)	**<0.001**
SCA, mm^2	0.28 ± 0.10 (0.26–0.30)	0.25 ± 0.08 (0.21–0.28)	0.26 ± 0.08 (0.23–0.30)	0.307
CVI (%)	41% ± 6.6% (39.8–42.8)	34.4% ± 9.5% (30.7–38.0)	39.7% ± 10.3% (35.9–43.6)	**0.001**
TCA, mm^2	0.48 ± 0.15 (0.45–0.52)	0.39 ± 0.09 (0.35–0.42)	0.45 ± 0.12 (0.40–0.50)	**0.007**

Significant *P* values are highlighted in bold.
CI = confidence interval; CVI = choroidal vascularity index; IIH = idiopathic intracranial hypertension; LCA = luminal choroidal area; ODD = optic disc drusen; SCA = stromal choroidal area; SD = standard deviation; TCA = total choroidal area..

thought to result from axoplasmic swelling and crowding of nerve fibers within the anatomically constrained prelaminar space. Consequently, the observed reductions in TCA, LCA, and CVI in eyes with papilledema may be partially explained by vascular compromise induced by mechanical compression.

In longitudinal comparisons of IIH patients before and after papilledema resolution, eyes with resolved papilledema demonstrated a mean increase in PPCVI relative to the acute phase, suggesting that choroidal vascular changes may occur after normalization of ICP. However, when comparing choroidal vascular parameters with those of the

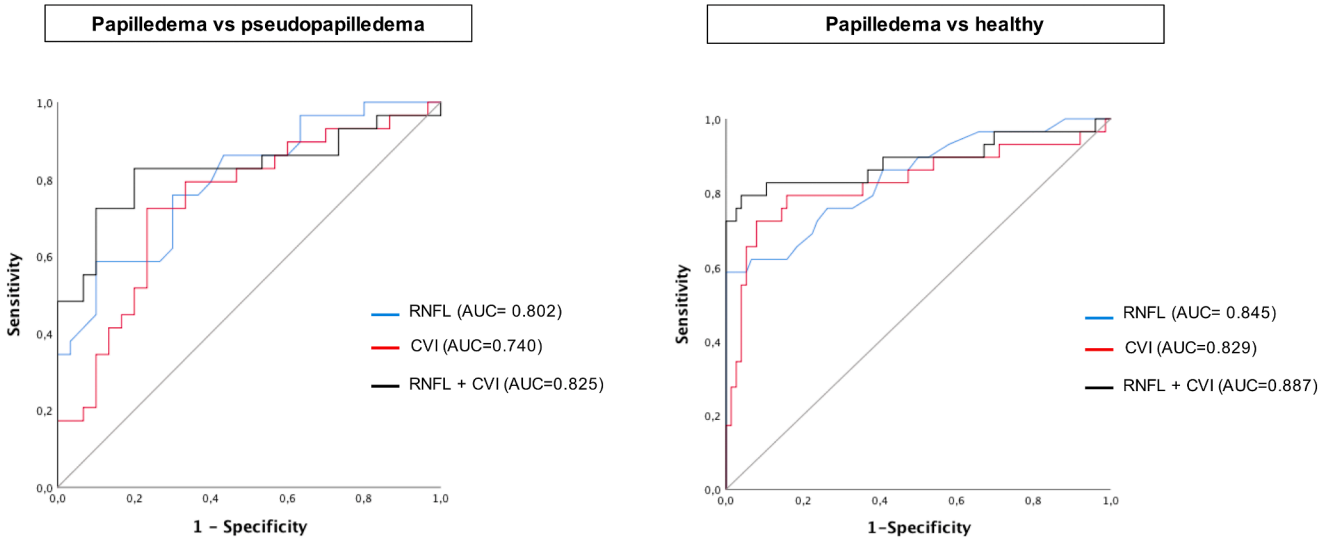

Figure 6. Receiver operating curve analysis to evaluate the diagnostic performance of mean retinal nerve fiber layer (RNFL) and mean peripapillary choroidal vascularity index (PPCVI) and their combined effect to differentiate papilledema from pseudopapilledema and healthy controls. AUC= area under the curve; CVI = choroidal vascularity index.

pseudopapilledema and control groups, TCA, LCA, and CVI remained significantly reduced in the papilledema group, even during the remission stage. These findings indicate that structural alterations in the peripapillary choroid may persist despite clinical resolution of papilledema. In papilledema, mechanical compression and sustained elevation of ICP may induce chronic vascular remodeling of the short posterior ciliary arteries, contributing to long-term thinning of the peripapillary choroid and decreased vascular density, even after the resolution of acute optic disc edema. In parallel, axonal degeneration and the consequent reduction in metabolic demand from the adjacent RNFL may lead to secondary reduction of the peripapillary choroidal vasculature. Together, these mechanisms may account for the persistently reduced choroidal vascular parameters observed in IIH patients during the remission phase, despite clinical resolution of papilledema.

The main limitation is the retrospective design of the study and the small sample size of patients included. Furthermore, in the present study, we did not find a correlation between the degree of papilledema and the reduction of the PPCVI. Another limitation is that patients with grade 1 and grade 5 papilledema were excluded. Grade 1 papilledema may be particularly difficult to distinguish from pseudopapilledema, whereas grade 4 papilledema often presents with pronounced swelling that may facilitate differentiation. Therefore, further research with larger cohorts is warranted to more accurately evaluate the relationship between papilledema grade and choroidal changes, to assess PPCVI in the early stages, and to elucidate the role of the choroid in the pathogenesis of papilledema. Furthermore, comparing choroidal changes across different causes of papilledema and pseudopapilledema would help in determining whether our findings can be generalized to all forms of papilledema or are primarily specific to the pathogenesis of IIH. Another limitation is that the deep learning model was used solely for segmentation and quantitative measurement of the peripapillary choroid, without performing direct diagnostic classification. Future research will focus on developing a deep learning–based diagnostic framework that integrates PPCVI, TCA, RNFL measurements, and clinical parameters to automatically differentiate papilledema from pseudopapilledema using single peripapillary OCT scans. Expanding the sample size will enable validation of the model and assessment of its clinical utility as a rapid, noninvasive tool for supporting diagnosis and monitoring disease progression.

Conclusions

Our findings support the hypothesis that a reduction in PPCVI may serve as a useful biomarker for distinguishing papilledema from pseudopapilledema. Additionally, the observed increase in PPCVI after the resolution of papilledema suggests its potential as a noninvasive parameter for monitoring disease progression and treatment response. Given the potential of deep learning for medical image analysis and the rich information contained within the choroidal region of OCT images, further studies are needed to confirm our results and gradually expand the application of deep learning algorithms in the daily clinical practice of optic nerve diseases.

Footnotes and Disclosures

Originally received: June 24, 2025.
Final revision: November 17, 2025.
Accepted: November 21, 2025.
Available online: November 28, 2025.Manuscript no. XOPS-D-25-00462.

[1] Ophthalmology Unit, Dipartimento di Scienze Mediche e Chirurgiche, Alma Mater Studiorum University of Bologna, Bologna, Italy.

[2] IRCCS Azienda Ospedaliero-Universitaria di Bologna, Bologna, Italy.

[3] Department of Ophthalmology, University of Pittsburgh School of Medicine, Pittsburgh, Pennsylvania.

Disclosures:
The authors have no proprietary or financial interest in any aspect of this report. The authors have no funding to report.

This work was supported by NIH CORE Grant P30 EY08098 to the Department of Ophthalmology, the Eye and Ear Foundation of Pittsburgh, and from an unrestricted grant from Research to Prevent Blindness, New York, NY.

Support for Open Access publication was provided by DIMEC Alma Mater Studiorum, University of Bologna.

Data availability statement: The datasets used and/or analysed during the current study are available from the corresponding author on reasonable request.

HUMAN SUBJECTS: Human subjects were included in this study. All procedures adhered to the principles of the Declaration of Helsinki, and all participants provided written informed consent. This study was approved by the Ethics Committee of Bologna, Italy (Cod CE: 53/2025/Oss/AOUBo).

No animal subjects were used in this study.

Author Contributions:

Conception and design: Valsecchi, Ibrahim, Schiavi, Vupparaboina, Chhablani, Fontana

Analysis and interpretation: Valsecchi, Padovani, Davis, Ibrahim, Vallone, Roda, Vupparaboina, Chhablani, Fontana

Data collection: Valsecchi, Davis, Ibrahim, Roda, Chhablani, Fontana

Obtained funding: N/A

Overall responsibility: Valsecchi, Padovani, Ibrahim, Roda, Mete, Moramarco, Schiavi, Vupparaboina, Chhablani, Fontana

Abbreviations and Acronyms:
AUC = area under the curve; **CIB** = choroidal inner boundary; **COB** = choroidal outer boundary; **CVI** = choroidal vascularity index; **ICP** = intracranial pressure; **IIH** = idiopathic intracranial hypertension; **LCA** = luminal choroidal area; **ODD** = optic disc drusen; **PPCVI** = peripapillary choroidal vascularity index; **RNFL** = retinal nerve fiber layer; **SD-OCT** = spectral-domain OCT; **TCA** = total choroidal area.

Keywords:
Peripapillary CVI, Choroid, Papilledema, Pseudopapilledema.

Correspondence:
Nicola Valsecchi, MD, Ophthalmology Unit, DIMEC, Alma Mater Studiorum University of Bologna, Italy, IRCCS Azienda Ospedaliero-Universitaria di Bologna, Via Pelagio Palagi 9, Bologna 40138, Italy. E-mail: nicola.valsecchi2@studio.unibo.it.

References

1. Xie JS, Donaldson L, Margolin E. Papilledema: a review of etiology, pathophysiology, diagnosis, and management. *Surv Ophthalmol*. 2022;67:1135−1159.
2. El-Gendy RS, El-Hamid ASA, Galhom AESA, et al. Diagnostic dilemma of papilledema and pseudopapilledema. *Int Ophthalmol*. 2024;44:272.
3. Friedman DI, Jacobson DM. Diagnostic criteria for idiopathic intracranial hypertension. *Neurology*. 2002;59:1492−1495.
4. Radhakrishnan K, Ahlskog JE, Cross SA, et al. Idiopathic intracranial hypertension (pseudotumor cerebri). Descriptive epidemiology in Rochester, Minn, 1976 to 1990. *Arch Neurol*. 1993;50:78−80.
5. Jivraj I, Cruz CA, Pistilli M, et al. Utility of spectral-domain optical coherence tomography in differentiating papilledema from pseudopapilledema: a prospective longitudinal study. *J Neuroophthalmol*. 2021;41:e509−e515.
6. Liu B, Murphy RKJ, Mercer D, et al. Pseudopapilledema and association with idiopathic intracranial hypertension. *Childs Nerv Syst*. 2014;30:1197−1200.
7. Chang MY, Binenbaum G, Heidary G, et al. Imaging methods for differentiating pediatric papilledema from pseudopapilledema: a report by the American academy of ophthalmology. *Ophthalmology*. 2020;127:1416−1423.
8. Chang MY, Heidary G, Beres S, et al. Artificial intelligence to differentiate pediatric pseudopapilledema and true papilledema on fundus photographs. *Ophthalmol Sci*. 2024;4:100496.
9. Sadeghi E, Valsecchi N, Rahmanipour E, et al. Choroidal biomarkers in age-related macular degeneration. *Surv Ophthalmol*. 2024;70:167−183.
10. Valsecchi N, Roda M, Febbraro S, et al. Choroidal morphology and microvascular structure in eyes of patients with idiopathic normal pressure hydrocephalus before and after ventriculo-peritoneal shunt surgery. *Sci Rep*. 2023;13:16379.
11. Kaya FS, Arici C. Assessment of peripapillary choroidal thicknesses and optic disc diameters in idiopathic intracranial hypertension. *Can J Ophthalmol*. 2023;58:212−218.
12. Kesim C, Solmaz B, Pasaoglu I, et al. Analysis of the peripapillary choroidal vascular characteristics in papilledema associated with Pseudotumor Cerebri. *Optom Vis Sci*. 2021;98:326−333.
13. Frisén L. Swelling of the optic nerve head: a staging scheme. *J Neurol Neurosurg Psychiatry*. 1982;45:13−18.
14. Malmqvist L, Bursztyn L, Costello F, et al. The optic disc Drusen studies consortium recommendations for diagnosis of optic disc Drusen using optical coherence tomography. *J Neuroophthalmol*. 2018;38:299−307.
15. Optical Coherence Tomography Substudy Committee, NORDIC Idiopathic Intracranial Hypertension Study Group. Papilledema outcomes from the optical coherence tomography substudy of the idiopathic intracranial hypertension treatment trial. *Ophthalmology*. 2015;122:1939−1945.e2.
16. Ibrahim MN, Bashar SB, Rasheed MA, et al. Volumetric quantification of choroid and Haller's sublayer using OCT scans: an accurate and unified approach based on stratified smoothing. *Comput Med Imaging Graphics*. 2022;99:102086.
17. Chen Q, Niu S, Fang W, et al. Automated choroid segmentation of three-dimensional SD-OCT images by incorporating EDI-OCT images. *Comput Methods Programs Biomed*. 2018;158:161−171.
18. Vupparaboina KK, Selvam A, Suthaharan S, et al. Automated choroid layer segmentation based on wide-field SS-OCT images using deep residual encoder-decoder architecture. *Invest Ophthalmol Vis Sci*. 2021;62:2162.
19. Vupparaboina KK, Richhariya A, Chhablani J, Jana S. *Optical coherence tomography imaging: automated binarization of choroid for stromal-luminal analysis*. 2016 International Conference on Signal and Information Processing (IConSIP), Nanded, India; 2016:1−5.
20. Girard MJA, Strouthidis NG, Ethier CR, Mari JM. Shadow removal and contrast enhancement in optical coherence tomography images of the human optic nerve head. *Invest Ophthalmol Vis Sci*. 2011;52:7738−7748.
21. Ibrahim MN, Bollepalli SC, Selvam A, et al. *Accurate detection of 3D choroidal vasculature using swept-source OCT volumetric scans based on Phansalkar thresholding*. Pittsburgh: 2023 IEEE EMBS International Conference on Biomedical and Health Informatics (BHI). IEEE; 2023:1−4.
22. Thompson AC, Bhatti MT, El-Dairi MA. Bruch's membrane opening on optical coherence tomography in pediatric papilledema and pseudopapilledema. *J AAPOS*. 2018;22:38−43.e3.
23. Chiu HH, Yang FP, VandenHoven C, Wan MJ. Utility of spectral domain OCT in differentiating optic disc drusen from papilledema in children. *Can J Ophthalmol*. 2021;56:250−255.
24. Fard MA, Fakhree S, Abdi P, et al. Quantification of peripapillary total retinal volume in pseudopapilledema and mild papilledema using spectral-domain optical coherence tomography. *Am J Ophthalmol*. 2014;158:136−143.
25. Sekhri R, Kuht HJ, Tu Z, et al. Identifying biomarkers for papilledema and pseudopapilledema. *Sci Rep*. 2025;15:24847.
26. Girard MJA, Panda S, Tun TA, et al. Discriminating between Papilledema and optic disc Drusen using 3D structural analysis of the optic nerve head. *Neurology*. 2023;100:e192−e202.
27. Tüntaş Bilen F, Atilla H. Peripapillary vessel density measured by optical coherence tomography angiography in idiopathic intracranial hypertension. *J Neuro-Ophthalmology*. 2019;39:319.
28. Hayreh SS. Segmental nature of the choroidal vasculature. *Br J Ophthalmol*. 1975;59:631−648.
29. Hayreh SS. Posterior ciliary artery circulation in health and disease: the Weisenfeld lecture. *Invest Ophthalmol Vis Sci*. 2004;45:749−757.
30. Mittra RA, Sergott RC, Flaharty PM, et al. Optic nerve decompression improves hemodynamic parameters in papilledema. *Ophthalmology*. 1993;100:987−997.
31. Paulson OB, Strandgaard S, Edvinsson L. Cerebral autoregulation. *Cerebrovasc Brain Metab Rev*. 1990;2:161−192.
32. Flaharty PM, Phillips W, Sergott RC, et al. Color doppler imaging of superior ophthalmic vein thrombosis. *Arch Ophthalmol*. 1991;109:582−583.
33. Hayreh SS. Pathogenesis of optic disc edema in raised intracranial pressure. *Prog Retin Eye Res*. 2016;50:108−144.